Composites: Part A 56 (2014) 44–50

Contents lists available at ScienceDirect

Composites: Part A

journal homepage: www.elsevier.com/locate/compositesa

Interface enhancement of carbon nanotube/mesocarbon microbead isotropic composites

Ke Shen [a], Qiang Zhang [b], Zheng-Hong Huang [a], Junhe Yang [c], Guangzhi Yang [c], Wanci Shen [a], Feiyu Kang [a,d,*]

[a] State Key Laboratory of New Ceramics and Fine Processing, School of Materials Science and Engineering, Tsinghua University, Beijing 100084, China
[b] Beijing Key Laboratory of Green Chemical Reaction Engineering and Technology, Department of Chemical Engineering, Tsinghua University, Beijing 100084, China
[c] School of Materials Science and Engineering, University of Shanghai for Science and Technology, Shanghai 200093, China
[d] City Key Laboratory of Thermal Management Engineering and Materials, Graduate School at Shenzhen, Tsinghua University, Shenzhen 518055, Guangdong, China

ARTICLE INFO

Article history:
Received 23 June 2013
Received in revised form 12 September 2013
Accepted 14 September 2013
Available online 21 September 2013

Keywords:
Mesocarbon microbeads
A. Carbon nanotube
B. Interfacial strength
E. Isostatic pressing

ABSTRACT

Carbon nanotubes (CNTs) are incorporated into mesocarbon microbead (MCMB)-derived isotropic graphite to improve their mechanical properties. CNTs are homogenously distributed on the MCMB surface by acid-treatment and mechanical mixing. The composites are prepared by cold isostatic pressing, carbonization, and graphitization. The mechanical properties and isotropy ratios of the CNT/MCMB composites are determined by four-point bend tests and thermal expansion measurements, respectively. The addition of CNTs improves the flexural strength by *ca.* 20%, while keeps a low isotropy ratio. CNTs dispersed on particle interfaces improve the interfacial strength, this reinforcing mechanism is confirmed by a fracture mode analysis with scanning electron microscope.

1. Introduction

Carbon and graphite materials are characterized by excellent mechanical performance at high temperatures, high electrical and thermal conductivity, and good corrosion resistance. Modern advanced technologies make wide use of polycrystalline graphite in different fields, including graphite electrodes used in electric arc furnaces, graphite cathodes in aluminum electrolysis cells, graphite dies used for continuous casting, fine-grain graphite heaters and crucibles used for single crystal silicon growth, and nuclear-grade graphite moderators in high-temperature reactors [1].

Polycrystalline graphite is usually prepared by two methods [2]. The first one makes use of pulverized coke as a filler and pitch as a binder. The other uses self-sintering carbonaceous mesophase such as mesocarbon microbeads (MCMBs) for binderless forming [3,4]. The strength of MCMB-derived graphite is determined by several factors, including pre-oxidation conditions, the degree of graphitization, as well as particle size distribution.

Pre-oxidation treatment significantly influences the pyrolysis behavior, and change the plasticity of carbonaceous mesophase. Many investigations have been carried out to optimize the pre-oxidation conditions [5] and to investigate the MCMB sintering mechanism [6,7].

The graphitization decreases d_{002} interlayer spacing and induces the growth of graphite layers. In another words, turbostratic structure gradually evolves into graphitic structure. Generally, the carbonized artifacts have much higher strength than the graphitized artifacts. For instance, Wu et al. [8] fabricated carbon blocks by using raw MCMBs with particle sizes of less than 5 μm. The blocks were carbonization at 900 °C and showed a flexural strength of 111 MPa.

The particle size distribution is another important factor that influences mechanical properties of MCMB-derived graphite. The decrease of mean particle size gives rise to higher strength. A remarkably high flexural strength of 100 MPa is available for graphite sample prepared from mesophase pitch powder with a mean particle size of 2.4 μm after graphitization at 2773 K [9]. However, green bodies with small particle sizes are very easy to crack during baking. As a result, it is of great interest to explore new methods that can increase the strength of MCMB-derived graphite while do not reduce the particle size.

In this contribution, MCMBs with a D50 value of 25.0 μm are used as raw material. These MCMBs have been successfully made into graphite blocks with a diameter of 60 mm [6] in our previous work. Here we demonstrate a new approach of using carbon nanotubes (CNTs) to reinforce the MCMB-derived graphite. Many researches have been carried out in order to incorporate CNTs into polymers [10–12], metals [13], and ceramics [14,15] to form

* Corresponding author at: State Key Laboratory of New Ceramics and Fine Processing, School of Materials Science and Engineering, Tsinghua University, Beijing 100084, China. Tel./fax: +86 10 6279 2911.
E-mail address: fykang@mail.tsinghua.edu.cn (F. Kang).

1359-835X/$ - see front matter © 2013 Elsevier Ltd. All rights reserved.
http://dx.doi.org/10.1016/j.compositesa.2013.09.008

advanced composites. The reasons we selected CNTs as additives is the excellent mechanical properties of CNTs [16] and its good chemical compatibility with graphite. Wu et al. [8] added CNTs into coal tar pitch to *in situ* produce CNT/MCMB powders, which were subsequently used as the starting material to prepare composite materials. However it is not easy to control the particle morphology and structure during the *in situ* synthesis of CNT/MCMB powder. Song et al. [17] prepared CNT reinforced MCMB based composites by one-step self-sintering, but limited information was reported on the microstructure and reinforcement mechanism. Herein, a similar method was employed to directly disperse CNTs on the outer surface of MCMBs (as illustrated in Fig. 1). The composite powders are pressed and sintered in order to produce a CNT/MCMB isotropic composite, in which CNTs are homogenously deposited at MCMB interface areas. The mechanism of mechanical strength increasing was also investigated in detail.

2. Materials and methods

2.1. Preparation of CNT/MCMB composite powder

MCMBs produced by China Steel Chemical Corporation, Taiwan, were lightly pre-oxidized under optimized conditions, which are not open, and were used as received. The basic information about the MCMBs can be found in our previous publication [6].

Aligned multi-walled carbon nanotubes (MWCNTs) [18,19] were grown on a vermiculite-based catalyst by fluidized bed catalytic chemical vapor deposition. CNTs with an outer diameter in the range of 7–12 nm, a length of *ca.* 10 μm, and a purity of 84.0 wt.% were synthesized. High magnification scanning electron microscopy (SEM) images indicate that the CNTs in the array possess good alignment (Fig. 2), which facilitates the CNT dispersion. The CNT arrays were treated in an acid mixture of 98% H_2SO_4 and 68% HNO_3 with a volume ratio of 3:1 at 90 °C for 20 min, in order to remove impurities and to create oxygen-containing functional groups on the CNT surface [20]. After acid treatment, the purity of CNTs can be increased to 97.5 wt.%. The CNTs were separated by centrifugation, and then ultrasonically dispersed in ethanol for 15 min. Attributed from its low toxicity, ethanol was chosen as solvent. Subsequently, 200 g MCMBs were added into the ethanol. The suspension was continuously ultrasonic-treated and stirred for 60 min and then vacuum dried at 70 °C. The morphology of CNTs on the MCMB surface was observed by SEM. A series of composite powders with various CNT weight contents of 0.0, 0.05, 0.1, 0.25, 0.4, 0.6, and 0.75 wt.% were prepared.

2.2. Cold isostatic pressing, carbonization, and graphitization

Cold isostatic pressing (CIP) was employed to form the green composite body of about 30 mm in diameter and 200 mm in length. Green bodies were carbonized at 1000 °C in N_2 flow. The graphitization was carried out in Ar gas in an intermediate frequency induction heating furnace. The samples were first heated at a constant power of 10 kW to 1000 °C and then heated at a rate of 10 °C/min up to 2800 °C. After holding for 1 h, the furnace chamber was naturally cooled to room temperature.

2.3. Characterization of CNT/MCMB composites

The final bulk density was measured based on Archimedes' principle. X-ray diffraction (XRD) patterns of the samples were recorded using a Rigaku D/max 2500 V diffractometer with Cu Kα radiation. The graphitized samples with various CNT contents were machined into specimens of 5 × 10 × 50 mm for four-point bend tests, which were performed in a Shimadzu Servopulser material testing machine. During the test, the crosshead moved at a speed of 1 mm/min, the inner and outer spans were 10 mm and 40 mm, respectively. SEM images of fracture surfaces were recorded and analyzed. The NETZSCH DIL 402 PC thermal dilatometer was used to measure the coefficient of thermal expansion (CTE) in the temperature range of 20–500 °C with a heating rate of 5 °C/min. For the thermal expansion measurements, specimens were machined along both the axial and radial directions, and the isotropy ratio is calculated as the ratio of the CTE along the two orthogonal directions.

3. Results and discussion

3.1. CNT dispersion

The most important factor in the preparation of CNT-reinforced composites is a good CNT dispersion, which indicates the fact that individual CNTs have to be distributed uniformly and well separated from each other. Fig. 3 is SEM images of the composite powders, indicating that CNTs can be homogenously dispersed at relatively low CNT contents, i.e. 0.05, 0.10, 0.25 wt.%. For 0.25 wt.% CNT content (Fig. 3 (d)–(f)), the MCMB surface is covered by a large amount of uniformly distributed CNTs due to physical adsorption. The length of CNTs is shortened to a few microns, and their alignment is also lost. For 0.4 wt.% or higher CNT content, CNT dispersion is no longer homogeneous, the aggregates can be observed in SEM images (Fig. 3(c)). The ethanol is not as well as toluene or DMF solvent to disperse the CNTs. Besides, rather than the bulk homogenous distribution in the whole matrix, the CNTs prefer to be located at the surfaces of graphite particles. Consequently, the CNT content herein is lower than some other reported polymer composites or CNT/carbon composites.

3.2. Mechanical and thermal properties of the composites

The flexural strength upon increasing CNT weight content is presented in Fig. 4(a). The graphite artifact prepared from the original MCMBs, which were not treated in ethanol, shows a flexural strength of 37.05 MPa. CNTs remarkably increase the strength

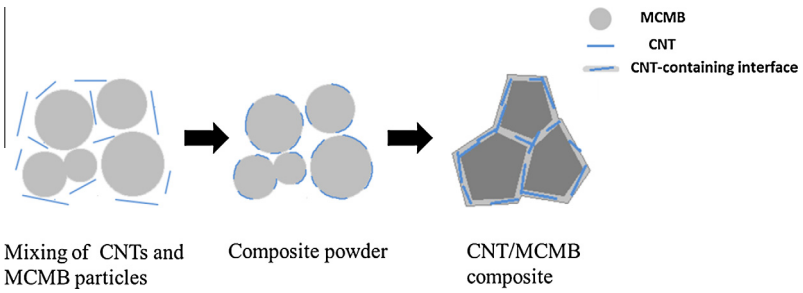

Fig. 1. Schematic of CNT/MCMB composite preparation. (For interpretation of the references to color in this figure legend, the reader is referred to the web version of this article.)

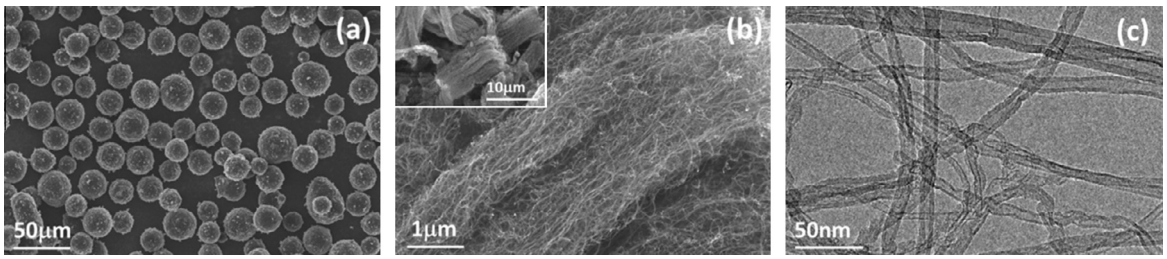

Fig. 2. Characterization of the raw materials. SEM image of (a) MCMB and (b) aligned CNTs. The inserted figure shows a low magnification SEM image of the aligned CNTs. (c) TEM image of MWCNTs.

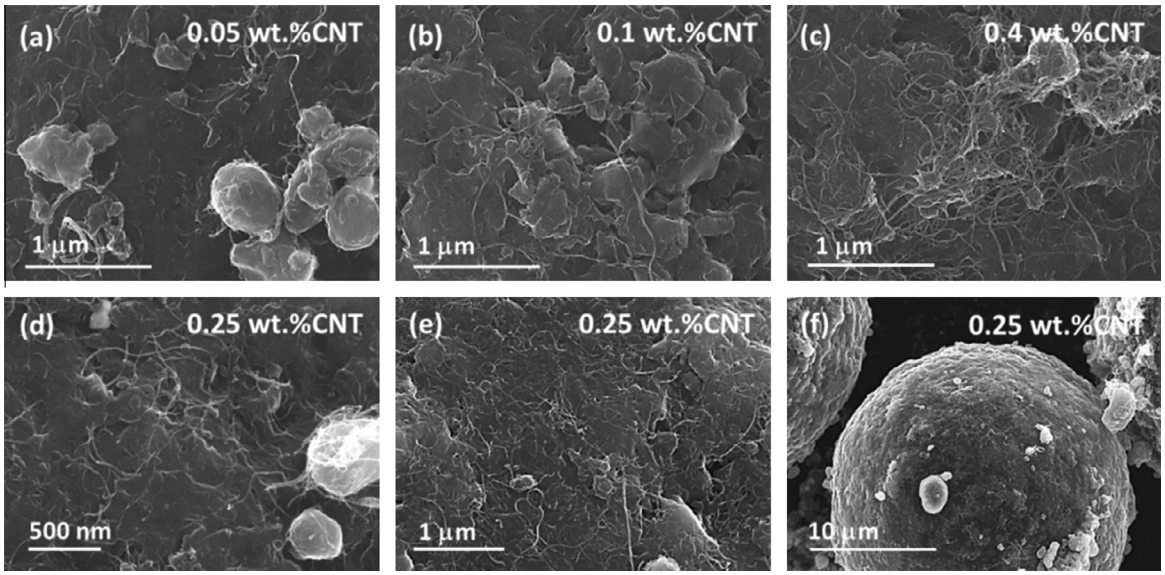

Fig. 3. SEM images of composite powders with various CNT weight contents. (a) 0.05 wt.%, (b) 0.1 wt.%, (c) 0.4 wt.%, and (d–f) 0.25 wt.% CNT content.

of the composite materials. The graphitized CNT/MCMB composite with addition of 0.25 wt.% CNTs, has a maximum average flexural strength of 44.38 MPa, corresponding to an increase of about 20%. The flexural strength of 0.4 wt.% CNT/MCMB composite decreases, which is attributed to the heterogeneous dispersion of CNTs. The figure inset in Fig. 4(b) compares the typical stress–strain curves of the raw MCMB-derived materials and the as-obtained composites. A region of linear elastic behavior was exhibited for every sample. The flexural modulus can be determined by the slopes. Song et al. [17,21] shows a modulus increase on CNT/mesophase pitch composite and a modulus decrease for CNT/MCMB composite. Herein, the flexural modulus in Fig. 4(b) changes upon CNT addition in a similar way as the strength illustrates as Fig 4(a). The modulus increase slightly below CNT addition of 0.25 wt.% and decrease as the CNT addition getting more than 0.4 wt.%.

In Fig. 5, each data point with error bar corresponds to an average density of eight specimens. Raw MCMB gives rise to a density of 1.796 g/cm^3. With the addition of a low amount of CNTs (less than 0.1 wt.%), the density evidently increases. The maximum density was determined at a CNT content of 0.1 wt.%. At higher CNT concentrations (more than 0.4 wt.%), porous CNTs aggregates generate inside the material, therefore decrease the composite density. Similar results have been reported by Deng et al. [22]. The aligned CNTs used in the current study have a mean wall number of 7.0 and a mean outside diameter of 9.4 nm [18]. According to the calculation by Laurent et al. [23], the density of these CNTs is *ca.* 2.0 g/cm^3. Thus, adding 0.1 wt.% of CNTs contributes very little to the experimentally observed density increase from 1.796 to 1.831 g/cm^3. A possible explanation should be better sintering or lower porosity caused by appropriate CNT content.

The mean CTE (100–500 °C) and the CTE-based isotropy ratio are listed in Table 1. Because of the random orientation of spherical particles, the composites have isotropic microstructure, the isotropy ratio of raw MCMB-derived graphite is as low as 1.02. After CNT addition, an isotropic ratio of 1.01 is available, in another words, CNTs do not influence the isotropic microstructure. However, the CTE value increases slightly owing to the change of microstructures.

3.3. Microstructure and fracture surface

Fig. 6 compares the XRD profiles of untreated CNTs, 0.25 wt.% CNT/MCMB composite powders, and the final graphitized composite. The diffraction pattern of untreated CNTs is characterized by a broad (002) and a small (10) reflection due to massive defects in carbon layers. In fact, (10) around 43° is the combination of (100) and (101). For the composite powders, the XRD profile mainly originates from MCMBs, since the amount of CNTs is too small to be detected. The composite specimen in bulk form was used to collect the XRD profile. After graphitization, the (002) reflection becomes very sharp and strong, (100) and (101) reflection separate clearly, and other diffraction peaks such as (004), (110), and (112) were observed, indicating a high degree of graphitization and a polycrystalline structure of graphite. Graphitization also removed the impurities in the composites.

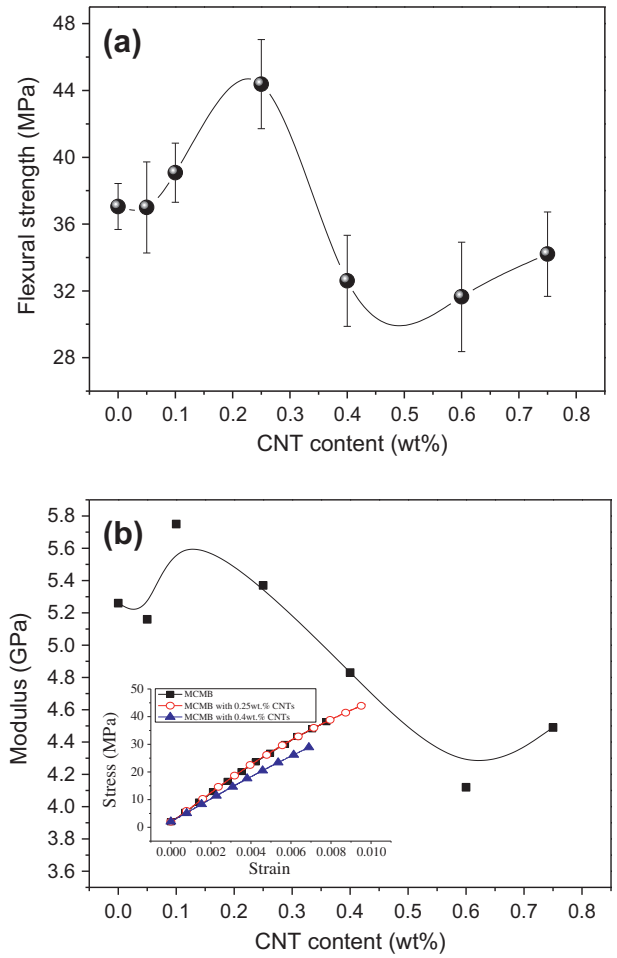

Fig. 4. (a) Effect of CNT content on flexural strength and (b) effect of CNT content on flexural modulus. Inset: stress–strain curves of raw MCMB-derived, 0.25 wt.%, and 0.4 wt.% CNT/MCMB composite materials. (For interpretation of the references to color in this figure legend, the reader is referred to the web version of this article.)

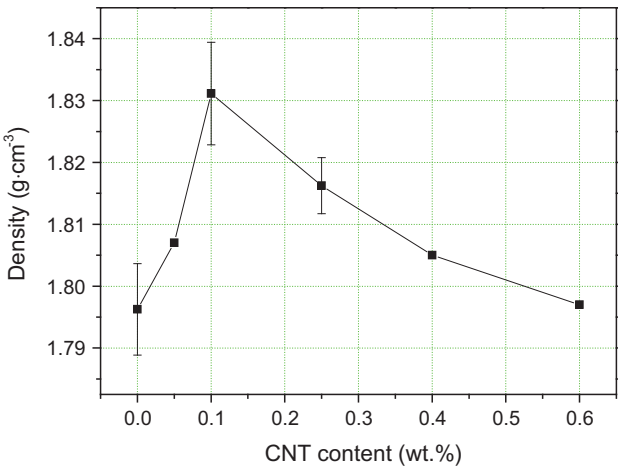

Fig. 5. Bulk density of CNT/MCMB composites. (For interpretation of the references to color in this figure legend, the reader is referred to the web version of this article.)

The fracture surface of binder-free MCMB-derived graphite is quite different from that of conventional polycrystalline graphite, which is composed of filler particles and binder phase. The easy identification of individual MCMB particles makes it possible to divide

Table 1
CTE and isotropy ratio of MCMB-derived graphites.

Sample	CTE (10^{-6}/K)		Isotropy ratio
	Axial	Radial	
Raw MCMB-derived graphite	6.06	6.17	1.02
0.25 wt.% CNT/MCMB composite	6.28	6.25	1.01

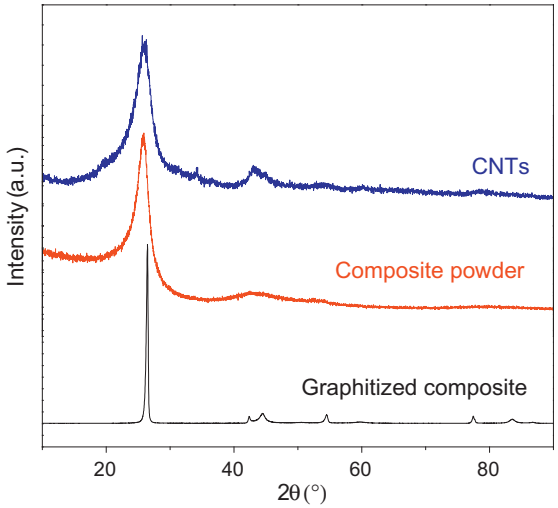

Fig. 6. XRD patterns of CNTs, 0.25 wt.% CNT/MCMB composite powder, and the graphitized composite. (For interpretation of the references to color in this figure legend, the reader is referred to the web version of this article.)

the fracture surface into three classes. Fig. 7(b) shows an intergranular fracture surface where the sphere morphology can be seen. However, in some areas where the interfacial strength is higher than the particle strength, innergranular fracture occurs instead of the intergranular mode. The innergranular fracture mode can be divided into two classes further, the cleavage fracture and the "edge-on" fracture mode, which are shown in Fig. 7(c) and (d). Fig. 7(c) shows a typical cleavage fracture surface, where a very smooth (002) plane can be observed. The cleavage occurs between (002) planes, because of the weak van der Waals force between graphite layers. In some cases, the cracks advance through the microbeads and cut the (002) planes in half, giving rise to "edge-on" cross-sections, as shown in the circles in Fig. 7(a). The "edge-on" fracture causes the C–C covalent bond dissociation which need much more energy than cleavage between the (002) planes. Fig. 7(d) provides the detailed morphology of the "edge-on" fracture surface. The fracture surface of raw MCMB-derived graphite was also examined. By comparison, the "edge-on" fracture mode is mostly observed in the 0.25 wt.% CNT/MCMB composite. This should be attributed to the interfacial bond strength increase. The detailed CNT reinforcing mechanism is proposed in the following section.

Since CNTs were introduced by mechanical mixing, they only distributed on the interface of MCMB particles. A similar microstructure was observed in CNT/ceramic composites [24,25]. Fig. 8 shows the CNT-containing surface, and confirms the existence of CNTs in the graphitized composites. The circle in Fig. 8(a) indicate a cleavage fracture surface. The homogenously dispersed CNTs near the cleavage fracture surface are clearly visible in Fig. 8(b). The partial fusibility of MCMBs at evaluated temperature facilitates the formation of CNT-containing interface during MCMB sintering. A high magnification SEM image (Fig. 8(c)) displays that CNTs are embedded in the interface, in this way, CNTs effectively increase the interfacial strength of MCMB particles.

Fig. 9 shows typical TEM images of the composite graphitized at 2800 °C. Fig. 9(a) gives some evidences of the CNT and graphite

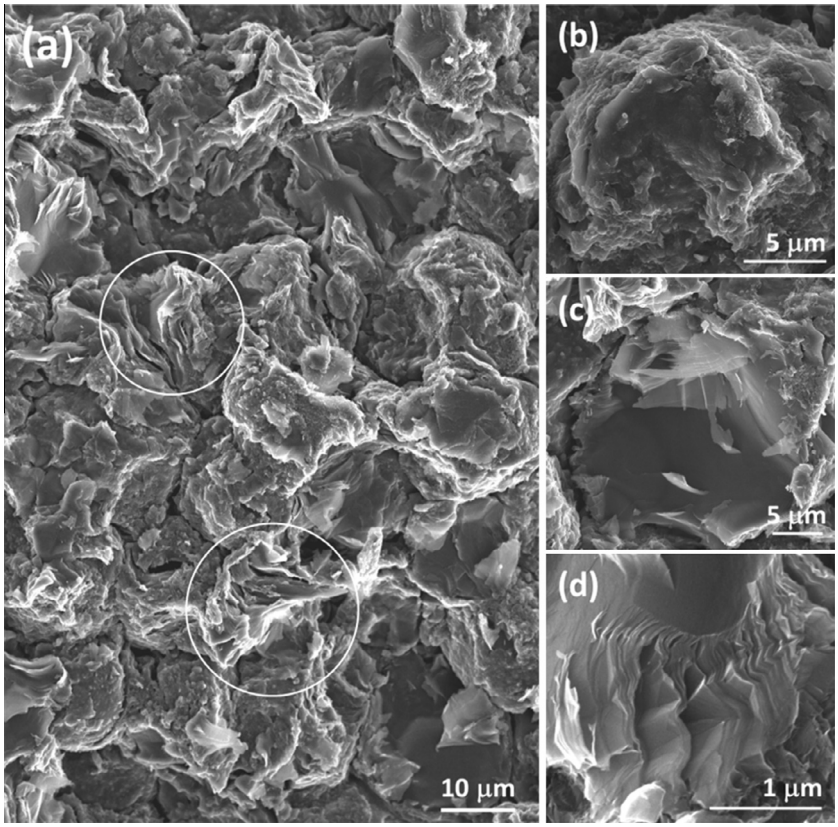

Fig. 7. SEM images of fracture surface of (a) 0.25 wt.% CNT/MCMB composite, and representative facture modes: (b) intergranular fracture mode, (c) cleavage fracture mode, and (d) "edge-on" fracture mode.

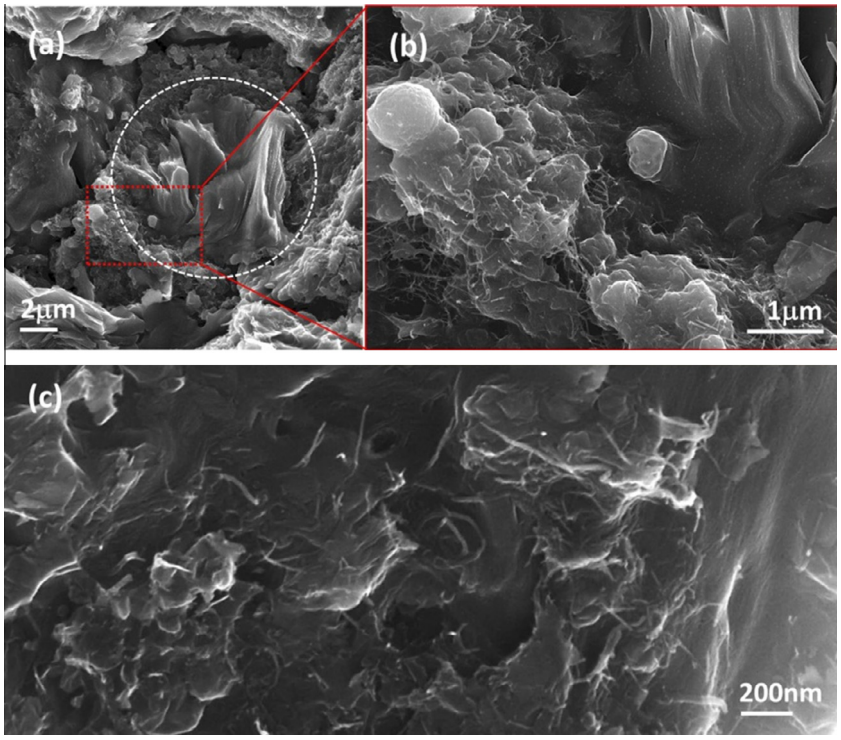

Fig. 8. SEM images of the CNT-containing interfaces. (For interpretation of the references to color in this figure legend, the reader is referred to the web version of this article.)

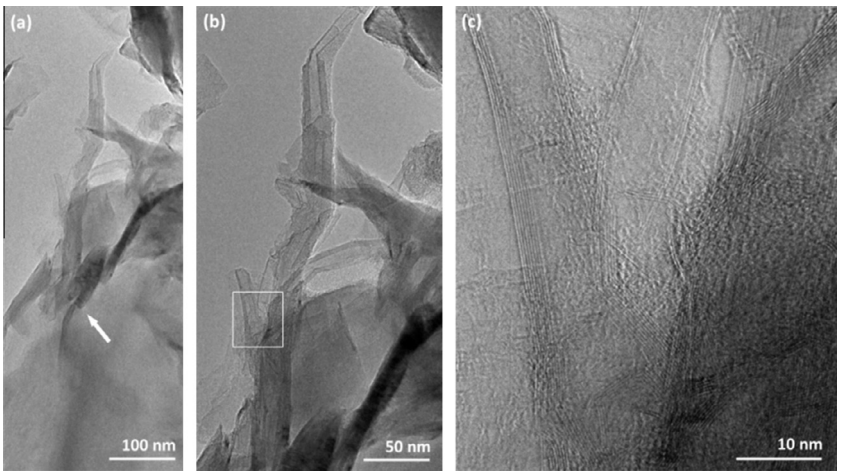

Fig. 9. TEM images of CNTs in the 2800 °C graphitized composite.

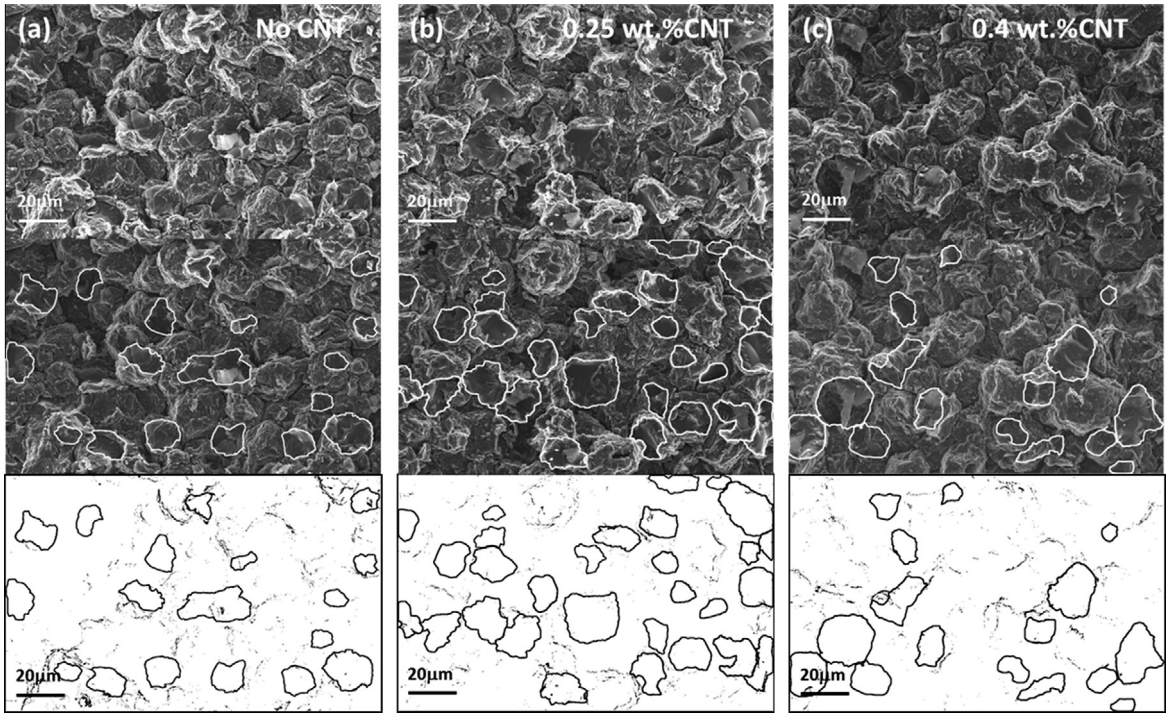

Fig. 10. Fracture surfaces of (a) raw MCMB-derived graphite, (b) 0.25 wt.% CNT/MCMB composite, and (c) 0.4 wt.% CNT/MCMB composite. Top: The original SEM images of the fracture surface. Middle: SEM images indicating the innergranular fracture mode (Cleavage fracture and "edge-on" fracture). Bottom: high contrast microstructure image showing the variation in the fracture surface type.

matrix interaction. A join is made between the CNT and graphite matrix. In Fig. 9(b), the CNT walls around the joints seem to be thick and irregular. Compared with the as-produced CNTs in Fig. 2(c), the CNT walls become straight because of the removal of small defects and the growth of graphite layers. However, gross defects in the CNTs are not removed. This is illustrated by curves along the graphitized CNTs in Fig. 9(b), and the 'kinked' walls shown in Fig. 9(c).

3.4. Reinforcing mechanism

The reinforcing mechanism is explained in terms of the strengthening effect of CNT-containing interfaces. This may conflict with the mechanism proposed for CNT/ceramic composites [26]. Wang et al. [27] and Vasiliev et al. [25] have concluded that the CNT bundles located at Al_2O_3 grain boundaries mechanically weaken the interface bonding. As a result, the fracture occurs at the grain boundaries (intergranular fracture). Considering CNT/MCMB composites, the CNT-containing particle interfaces exhibit a different mechanical behavior. Firstly, individual CNTs are homogeneously distributed at particle interfaces. Secondly, CNTs have very good chemical compatibility with the graphite matrix. Therefore, they are able to enhance the interfacial bond strength.

Evidence confirming this hypothesis is given by SEM observations of the fracture surfaces in Fig. 10. CNTs change the fracture mode of MCMB, which is mainly determined by the difference in the interfacial strength relative to the beads themselves. Obviously, innergranular fracture indicates a firmer bond or higher

interfacial strength compared to intergranular fracture. Thus, the interfacial bond situation can be reflect in the proportion of innergranular fracture surface.

Although the facture surfaces are rough, different fracture modes described in Fig. 7 can be easily distinguished due to their distinct appearance. The innergranular fracture surfaces (corresponding to Fig. 7(c) and (d)) are carefully selected with white lines in Fig. 10 for raw MCMB-derived graphite, 0.25 wt.% CNT/MCMB composite, and 0.4 wt.% CNT/MCMB composite, respectively. The areas of the circled regions (Fig. 10 bottom) are measured as 13.2%, 24.9% and 14.7%, which stand for the fraction of the innergranular fracture surface. With addition of CNTs, the innergranular fracture mode increases remarkably due to higher interfacial strength, then decreases due to CNT aggregation, showing the same variation as the flexural strength upon increasing CNT content. Therefore, it is reasonable to attribute the strengthening effect to the CNT-containing interface reinforcement.

4. Conclusion

The CNT/MCMB isotropic composites with improved mechanical properties were prepared. CNTs were uniformly dispersed by an acid treatment and incorporated onto the MCMB surface by physical adsorption. CNT-containing interfaces were obtained with the aid of MCMB sintering. The strength and modulus firstly increase and then decrease upon CNT addition. Composites with 0.25 wt.% CNTs showed a slight increase in the bulk density and an increase of *ca.* 20% in the flexural strength. Besides, the addition of CNTs did not influence the CTE-based isotropy ratio. The fracture mode of MCMB particle can be classified into three types, including intergranular fracture, cleavage fracture, and "edge-on" fracture mode. The CNT-containing interface plays an important role in the reinforcing mechanism as the CNTs increases the interfacial bond strength. This finding was supported by an increase in the fraction of innergranular fracture surface, which were observed in the 0.25 wt.% CNT/MCMB composite.

References

[1] http://www.sglgroup.com/cms/international/applications/index.html?__locale=en.
[2] Wang YG, Korai Y, Mochida I. Carbon disc of high density and strength prepared from synthetic pitch-derived mesocarbon microbeads. Carbon 1999;37(7):1049–57.
[3] Hoffmann WR, Huttinger KJ. Sintering of powders of polyaromatic mesophase to high-strength isotropic carbons. 1. Influence of the raw-material and sintering conditions on the properties of the carbon materials. Carbon 1994;32(6):1087–103.
[4] Norfolk C, Mukasyan A, Hayes D, McGinn P, Varma A. Processing of mesocarbon microbeads to high-performance materials: part I. Studies towards the sintering mechanism. Carbon 2004;42(1):11–9.
[5] Fanjul F, Granda M, Santamaria R, Menendez R. Optimization of the preparation conditions of polygranular carbons from mesophase. J Mater Sci 2003;38(3):427–35.
[6] Shen K, Huang ZH, Yang JH, Shen W, Kang FY. Effect of oxidative stabilization on the sintering of mesocarbon microbeads and a study of their carbonization. Carbon 2011;49(10):3200–11.
[7] Zhou CJ, McGinn PJ. The effect of oxygen on the processing of mesocarbon microbeads to high-density carbon. Carbon 2006;44(9):1673–81.
[8] Wu B, Wang Z, Gong QM, Song HH, Liang J. Fabrication and mechanical properties of in situ prepared mesocarbon microbead/carbon nanotube composites. Mater Sci Eng A 2008;487(1–2):271–7.
[9] Fujiura R, Kojima T, Komatsu M, Mochida I. Mechanical properties of binderless carbon mould prepared from heat-treated mesophase pitch of controlled grain size. Carbon 1995;33(8):1061–8.
[10] Coleman JN, Khan U, Gun'ko YK. Mechanical reinforcement of polymers using carbon nanotubes. Adv Mater 2006;18(6):689–706.
[11] Spitalsky Z, Tasis D, Papagelis K, Galiotis C. Carbon nanotube-polymer composites: chemistry, processing, mechanical and electrical properties. Prog Polym Sci 2010;35(3):357–401.
[12] Jia XL, Zhang Q, Zhao MQ, Xu GH, Huang JQ, Qian WZ, et al. Dramatic enhancements in toughness of polyimide nanocomposite via long-CNT-induced long-range creep. J Mater Chem 2012;22(14):7050–6.
[13] Bakshi SR, Lahiri D, Agarwal A. Carbon nanotube reinforced metal matrix composites – a review. Int Mater Rev 2010;55(1):41–64.
[14] Cho J, Boccaccini AR, Shaffer MSP. Ceramic matrix composites containing carbon nanotubes. J Mater Sci 2009;44(8):1934–51.
[15] Peigney A. Composite materials: tougher ceramics with nanotubes. Nat Mater 2003;2(1):15–6.
[16] Baughman RH, Zakhidov AA, de Heer WA. Carbon nanotubes – the route toward applications. Science 2002;297(5582):787–92.
[17] Song YZ, Li SZ, Zhai GT, Shi JL, Guo QG, Liu L, et al. Mechanical and physical properties of MWCNT/carbon composites with matrix derived from mesocarbon microbeads. Carbon 2008;46(7):1100–2.
[18] Zhang Q, Zhao MQ, Huang JQ, Liu Y, Wang Y, Qian WZ, et al. Vertically aligned carbon nanotube arrays grown on a lamellar catalyst by fluidized bed catalytic chemical vapor deposition. Carbon 2009;47(11):2600–10.
[19] Zhang Q, Zhao MQ, Huang JQ, Nie JQ, Wei F. Mass production of aligned carbon nanotube arrays by fluidized bed catalytic chemical vapor deposition. Carbon 2010;48(4):1196–209.
[20] Wang Y, Wu J, Wei F. A treatment method to give separated multi-walled carbon nanotubes with high purity, high crystallization and a large aspect ratio. Carbon 2003;41(15):2939–48.
[21] Song YZ, Zhai GT, Shi JL, Guo QG, Liu L. Carbon nanotube: carbon composites with matrix derived from oxidized mesophase pitch. J Mater Sci 2007;42(22):9498–500.
[22] Deng CF, Wang DZ, Zhang XX, Li AB. Processing and properties of carbon nanotubes reinforced aluminum composites. Mater Sci Eng A 2007;444(1–2):138–45.
[23] Laurent C, Flahaut E, Peigney A. The weight and density of carbon nanotubes versus the number of walls and diameter. Carbon 2010;48(10):2994–6.
[24] Zapata-Solvas E, Gomez-Garcia D, Dominguez-Rodriguez A. On the microstructure of single wall carbon nanotubes reinforced ceramic matrix composites. J Mater Sci 2010;45(9):2258–63.
[25] Vasiliev AL, Poyato R, Padture NP. Single-wall carbon nanotubes at ceramic grain boundaries. Scr Mater 2007;56(6):461–3.
[26] Padture NP. Multifunctional composites of ceramics and single-walled carbon nanotubes. Adv Mater 2009;21(17):1767–70.
[27] Wang XT, Padture NP, Tanaka H. Contact-damage-resistant ceramic/single-wall carbon nanotubes and ceramic/graphite composites. Nat Mater 2004;3(8):539–44.